Phase Referenced Stellar Interferometry at the Palomar Testbed Interferometer

Benjamin F. Lane

Department of Geological & Planetary Sciences, 150-21, California Institute of Technology, Pasadena, CA. 91125

ben@gps.caltech.edu

M. Mark Colavita

Jet Propulsion Laboratory, California Institute of Technology, 4800 Oak Grove Dr., Pasadena, CA., 91109

mcolavit@huey.jpl.nasa.gov

(for the PTI Collaboration)

ABSTRACT

We discuss implementation and testing of phase referencing at the Palomar Testbed Interferometer (PTI). A new instrument configuration provides a coherent integration of 10 or 20 milliseconds on a bright star while stabilizing the fringe phase of a nearby (20 arcseconds) and faint visual companion, allowing coherent integration times of at least 250 milliseconds. Observations have been made of several visual binaries, including 16 Cyg AB ($m_K = 4.5$ and 4.6) and HD 173648/173649 ($m_K = 4.3$ and ~ 5) to test the performance of the technique. These measurements also demonstrate that phase-referenced visibility measurements can be calibrated at the level of 3–7%.

Subject headings: instrumentation:interferometers–techniques:interferometric

1. Introduction

The sensitivity of a stellar interferometer is limited by the requirement that sufficient photons be collected in a coherence volume ($\tau_0 r_0^2$) to allow an accurate measurement of the fringe phase, and thus to allow fringe tracking. At the Palomar Testbed Interferometer (PTI, Colavita et al. 1999) the atmospheric coherence time (τ_0) in the K band (2.2 μm) is typically 10–20 ms, and the atmospheric coherence diameter (r_0) is $\sim$ 40 cm. This results in an effective tracking limit in dual-star mode (see below) of $m_K \simeq 4.5$, which limits the number of available targets. Phase referencing is a technique intended to improve the limiting magnitude of an interferometer. We report here the first results from testing of phase referencing at PTI.

If a star is too faint to track but appears close in the sky to a brighter star which can be tracked, the usual tracking limit no longer applies (Shao & Colavita 1992a; Quirrenbach et al. 1994). In this case one can use the measured fringe phase of the bright star to correct, in real time, the fringe phase of the fainter star. This effectively increases the atmospheric coherence time as seen by the second fringe tracker, allowing it to use a longer coherent integration time with a correspondingly fainter tracking limit. For the technique to work well the two stars must be separated by less than an isoplanatic angle, i.e., the angle on the sky over which atmospherically induced motion is well correlated ($\theta_i \propto r_0/h^*$, where h^* is the effective height of the turbulence profile, usually $\theta_i \sim 20$ arc-sec in the K band).

A major use of this technique will be narrow-angle astrometry (Shao & Colavita 1992b; Colavita et al. 1994), which allows one to detect fringes simultaneously on two closely spaced stars, and which can allow astrometric accuracy on the order of tens of micro-arcseconds. Although this type of measurement can be done without the use of phase referencing, the number of suitable target pairs may be quite small (for PTI with two 40-cm apertures: two stars brighter than 4.5 magnitudes and separated by less than 20 arc-seconds within the field of regard of the instrument, which results in $\sim$ 4 pairs). However, the situation improves considerably if one can use phase referencing to allow fainter reference stars. Thus phase referencing is required for narrow-angle astrometry to be used on a large scale, particularly in planet searches such as those planned for the Keck Interferometer.

2. Instrument Configuration

PTI was designed with an unusual "dual-star" configuration in which the image planes of the apertures can be split (usually by a 50-50 beamsplitter, although a pinhole can be used) such that light can be directed down two different beam paths to two separate beam combiners. Thus it is in effect two independent two-aperture interferometers that share the same apertures. Usually one star (the "primary") is observed on-axis, while the "secondary" star can be anywhere within an annulus with inner radius $\sim$ 8 arcseconds (closer than that and the tip-tilt sensor confuses the primary and secondary stars) and an outer radius of 1 arc minute.

After tip-tilt correction by a fast steering mirror, the starlight from each aperture passes through optical delay lines to correct for geometric and atmospheric optical path-length differences. PTI was designed such that both the primary and secondary starlight beams pass through a common long delay line ("LDL", capable of up to ± 38.3 m of optical delay), after which only the primary beam passes through a short delay line ("SDL", ± 3 cm of optical delay, corresponding to ± 1 arc-minute on the sky). In effect, the primary fringe tracker sees a "primary" delay line with an optical delay given by $\delta_p = \delta_{LDL} + \delta_{SDL}$, while the secondary fringe tracker sees a "secondary" delay line with delay $\delta_s = \delta_{LDL}$. The delay line controller orthogonalizes the commands sent to the physical delay lines such that the fringe trackers can request optical pathlength changes to the primary and secondary delay lines independently. Also, delay modulation (see below) can be applied to either or both of the delay lines.

Optical path-lengths are monitored by several laser metrology gauges, including independent LDL and SDL monitors, as well as a "constant-term" (CT) metrology system, which measures the total difference in optical path delay between the primary and secondary beams throughout the entire optical system out to the apertures. The SDL can use either its local metrology system or the CT to determine position. The latter case provides a way to compensate for piston vibrations of the optics in the starlight path and is used in phase referencing.

PTI is able to operate in three fundamental modes: the simplest is the case when only one fringe tracker operates, tracking and measuring the visibility of a single star. In this mode the 50-50 beamsplitters in the focal planes of the apertures are usually removed, increasing the photon throughput of the instrument. The second observing mode is used for astrometric measurements of similar-magnitude visual binary systems: in this mode both the primary and secondary fringe trackers operate independently with short sample times, and the primary and secondary delay lines are effectively independent. The third observing mode uses phase-referencing, in which the primary fringe tracker tracks a bright ($m_K < 4.5$) star with short sample times, while correcting the measured phase error for both the primary and secondary delay lines. In this mode the secondary fringe tracker can operate with integration times of 100 ms or longer.

3. Fringe Tracking & Phase Referencing

Fringe tracking at PTI (Colavita et al. 1999; Colavita 1999b) is implemented as follows: the tip-tilt corrected and delay-compensated starlight beams from each aperture are combined at a 50-50 beamsplitter. The output of the beamsplitter is two combined beams, one of which is focused directly onto a single pixel of a NICMOS-3 detector. This channel is usually operated in the astronomical K band ($2.0 - 2.4\ \mu$m), and is referred to as the "white-light" channel. The other beam is first spatially filtered by passage through a single-mode fiber and then dispersed with a prism before being focused onto 5–10 pixels (depending on the chosen spectral resolution, typically 65 nm/pixel) on the same detector, and is used as a spectrometer.

The fringe signal is measured by modulating the delay in a sawtooth pattern with an amplitude of one wavelength, and synchronously reading out the detector. For normal operation two sample times are available (10 and 20 ms), while for phase-referenced operation the secondary fringe tracker was modified to allow integration times of 50, 100 and 250 ms. During each sample the detector is first reset, a bias level is read, and then 4 reads are done, one after each quarter-wavelength of modulation. Denoting the integrated intensities in each $\lambda/4$ bin as A, B, C and D, the fringe quadratures are calculated as

$$X = A - C \tag{1}$$

$$Y = B - D \tag{2}$$

and the total flux as

$$N = A + B + C + D \tag{3}$$

After these quantities have been corrected for read-noise and detector biases for each pixel and frame, the fringe visibility is calculated as

$$V^2 = \frac{\pi^2}{2}\frac{X^2 + Y^2}{N^2} \tag{4}$$

and the fringe phase is found from

$$\phi = \tan^{-1}\frac{Y}{X} \tag{5}$$

This measured phase is "unwrapped" about a Kalman-filter based prediction to provide the phase used by the real-time system.

Once a new phase measurement becomes available, the fringe tracker adjusts the delay line position to keep the fringe phase as close to zero as possible. In practice this is done via an integrating servo (see Appendix A), and as is the case in any servo system, the correction is not perfect. In particular, the fringe tracker cannot control phase errors at frequencies above the servo bandwidth. Given a phase disturbance (the atmosphere) with power spectral density (PSD) $A(f)$, the PSD of the residual phase not corrected by the fringe tracker is given by

$$W(f) = A(f)H_{fb}(f) \tag{6}$$

where $H_{fb}(f)$ is the error (power) rejection of the servo

$$H_{fb}(f) \simeq \frac{1}{1 - 2\frac{f_c}{f}\mathrm{sinc}(\pi f T_s)\sin(2\pi f T_d) + \left(\frac{f_c}{f}\right)^2 \mathrm{sinc}^2(\pi f T_s)} \quad (7)$$

where $\mathrm{sinc}(x) = \sin(x)/x$, f_c is the closed-loop bandwidth of the servo, and T_s and T_d are delays (defined below). For the servo to be stable (not oscillate) the servo gain must be less than unity; typically $f_c \sim 0.1 - -0.21/T_s$. At PTI, $f_c \sim 5$ Hz for 20 ms sample times. T_s is the integration time of the measurement, effectively 15 ms for a sampling time of 20 ms (the lost time is due to modulation retrace and detector reset and settle time). T_d is the effective delay between measurement and correction, including data age. For PTI $T_d = 21.5$ ms for 20 ms sample times. The observed and theoretical servo responses are shown in Figs. 2 and 3.

Under good seeing conditions the primary fringe tracker can maintain a stable lock on a star for several minutes. Typical uncalibrated visibilities (V^2) in the spectrometer, which includes a spatial filter, are 0.7–0.8 when observing a point source. For the broad-band ("white-light") channel, which does not include a spatial filter, typical uncalibrated visibilities are 0.3–0.4.

With a fringe-tracking interferometer such as PTI, the most obvious way to implement phase referencing is simply to apply the delay corrections from the primary fringe tracker to both the primary and secondary delay lines; we call this the "feedback" approach. In this case we expect the power spectrum of the phase seen by the secondary beam combiner to look like the residual phase $W(f)$. Figure 1 shows how the unwrapped fringe phase is affected by the atmosphere, and how phase referencing stabilizes it. Figure 2 shows the power spectra of the same two cases, along with the best-fit atmospheric power spectrum. Also shown is the predicted power spectrum, based on application of Eq. 7 to the best-fit atmospheric power spectrum.

Although the feedback approach works well it is possible to do better. This comes about because the secondary delay line is not in the feedback path of the primary fringe tracker. Therefore there is no issue of servo stability, and the primary fringe tracker can apply all of the measured phase error to the secondary delay line, resulting in improved performance. We refer to this as the "feedforward" approach. In this case the error (power) rejection function is given by the feedback filter function, multiplied by a factor that depends only on the integration time and the time delay between the phase measurement and the application of the correction. (see Appendix A for a derivation)

$$H_{ff}(f) = H_{fb}(f)\left(1 - 2\mathrm{sinc}(\pi f T_s)\cos(2\pi f T_{ds}) + \mathrm{sinc}^2(\pi f T_s)\right) \quad (8)$$

The predicted power spectra of the secondary phase, based on the PSD filter functions and the model atmosphere power law of Fig. 2, is plotted in Fig. 4. As can be seen in the figure, using a feedforward servo the power at low frequencies falls off rapidly, and hence for sufficiently long integration times the feedforward case is expected to result in significantly reduced servo error compared to the feedback case. However, the slight increase in energy near f_c does mean that for short integration times (less than 100 ms) the feedback approach is to be preferred; our results are based on the feedback approach.

4. Visibility Reduction

One of the most important performance-limiting factors in phase-referencing is that fluctuations in the fringe position during integration reduce the measured fringe visibility ("smearing" the fringe). This reduction in V^2 can be calculated as (Colavita 1999b)

$$V_{sys}^2 = \exp[-(\sigma_\phi)_{hp}^2] \tag{9}$$

where $(\sigma_\phi)_{hp}^2$ is the high-pass filtered fluctuation of the phase about the interval mean

$$(\sigma_\phi)_{hp}^2 = \int_0^\infty W(f)[1 - \mathrm{sinc}^2(\pi f T)]df \tag{10}$$

where $W(f)$ is the power spectral density of the residual phase and T is the integration time. We calculated the expected reduction in fringe visibility for the theoretical feedback and feedforward servo filter functions applied to the best-fit model atmosphere of Figure 3. The results are shown in Fig. 4. We also note that these performance estimates are made based on the response time of the PTI systems; increasing fringe tracker bandwidth can reduce the loss of fringe visibility considerably (Fig. 6). However, increasing the fringe tracker bandwidth requires both faster computers and shorter integration times, which in turn necessitates either larger apertures or brighter reference stars.

5. Observations

An example of the visibility data produced by the instrument is given in Figure 6. In this experiment the primary fringe tracker continuously tracked 16 Cyg A, providing phase-referencing for the secondary fringe tracker. The secondary FT used a coherent integration time of 100 ms, and switched between observing 16 Cyg A and 16 Cyg B every 130 seconds. In each case we considered only the broadband white-light channel, as the narrowband spectrometers differed significantly between the two fringe trackers (the primary side includes a spatial filter while the secondary side uses a slit) complicating comparisons of measurement precision. As both 16 Cyg A and B are expected to appear as point sources (the radial velocity companion of 16 Cyg B (Cochran et al. 1997) is far too faint to be directly observed by PTI), we would expect to see a visibility given by (Boden et al. 1998)

$$V^2 = \left[\frac{2\ J_1(\pi B \theta / \lambda)}{\pi B \theta / \lambda} \right]^2 \tag{11}$$

where J_1 is the first-order Bessel function, B is the projected baseline vector magnitude at the star position, θ is the apparent angular diameter of the star, and λ is the center-band wavelength of the interferometer. This model predicts a constant visibility at a level determined by the angular size of the source, wavelength of observation, and projected baseline length of the interferometer.

The scatter (defined as $\sigma_{V^2} = \langle |V_i^2 - \langle V^2 \rangle | \rangle$) around a flat line is $\sim$ 18% for the uncalibrated phase-referenced data. However, notice that the fluctuations in visibility are common to both the primary (A) and secondary (B) stars - making it possible to calibrate the data by using measurements of star A to calibrate measurements of star B (as done routinely to calibrate non-phase-referenced data). This is done by assuming a uniform-disk model for the star A, and comparing the model visibility of the primary to the observed visibility of that star. From this one can derive the "system visibility" or inherent visibility response of the instrument ($V^2_{sys} = V^2_{raw,calibrator}/V^2_{model}$). The calibrated data is found by applying $V^2_{calibrated,target} = V^2_{raw,target}/V^2_{sys}$.

In addition to calibrating the observed fringe visibilities by interleaving observations of target and calibrators, the use of phase referencing means that there are simultaneous observations of the primary star by the "primary" fringe tracker; this makes possible a second approach to calibrating the data. As can be seen in Fig. 7, the fringe visibility measured by the primary fringe tracker is higher than that measured by the secondary fringe tracker, reflecting differences in both integration time and inherent instrumental response (due to a variety of differences in optical quality, alignment, and instrument layout). Nevertheless, it is evident from the figure that short-term changes in system visibility are somewhat correlated (a linear correlation coefficient r = 0.75), as might be expected from the fact that both systems are looking through (nearly) the same atmospheric turbulence. Hence it is possible to use the calibrator visibility measured by the primary fringe tracker to estimate the system visibility (V^2_{sys}). However, in this case it becomes necessary to assume (or measure via other means) an additional time-independent calibration factor, corresponding to the mean ratio of primary and secondary fringe tracker system visibilities.

In order to characterize the precision with which we can calibrate the phase-referenced visibility measurements by either of the above methods, a uniform-disk model was fit to the

Object	m_K	Date MJD	Coherent Int. Time (ms)	σ_{V^2} Sec. Cal.	Pri. Cal.	# Data Points	Estimated Diameter (mas)
61 Cyg B	2.8	51394.31	20	0.051	0.054	49	1.94 ± 0.009
		51365.48	100	0.040	0.034	12	2.14 ± 0.091
		51364.47	250	0.050	0.013	2	1.98 ± 0.319
		51410.31	250	0.025	0.030	8	2.14 ± 0.169
16 Cyg B	4.6	51365.42	100	0.069	0.049	12	0.96 ± 0.35
HD 173649	~ 5	51396.21	250	0.047	0.031	4	0.73 ± 0.22

Table 1: Measured scatter of the calibrated visibilities around a uniform-disk model, as measured by the secondary fringe tracker. Two different calibration schemes were tested: "Sec. Cal" refers to the case where visibility measurements were calibrated using interleaved measurements of a calibrator star, measured with the same (secondary) fringe tracker. "Pri. Cal." refers to data calibrated using simultaneous visibility measurements of the calibrator star using a different (primary) fringe tracker. Note that the 20 ms data was not phase-referenced, but is included to provide a comparison of data quality. Each data point corresponds to an incoherent averaging time of 130 seconds. The resulting diameter measurements can be compared to estimates derived from effective temperatures and bolometric fluxes based on archival broad-band photometry: $\theta_{61CygB} = 1.97 \pm 0.03$, $\theta_{16CygB} = 0.551 \pm 0.05$, and $\theta_{HD173649} = 0.3 \pm 0.05$ (all in milli-arcseconds).

calibrated data for several sources and integration times (see Table 1). The scatter of the measurements around the model, $\sim$ 3–7 %, are fully comparable with non-phase-referenced performance on much brighter sources. It appears that using the primary fringe tracker as a calibration reference does a comparable job of reducing the scatter in the visibilities. However, this method may be prone to systematic errors in estimating the ratio of system visibilities, and hence we suggest that a hybrid approach that makes use of both types of calibration may be preferable. For instance, one could use the primary fringe tracker to estimate short-term (second to minute timescales) fluctuations in V_{sys}, while using observations of the primary star with the secondary fringe tracker to establish the mean difference in V_{sys} between the two fringe trackers. By making use of the information provided by the primary fringe tracker in this manner one can reduce the number of calibration observations required.

6. Conclusion

By synthetically increasing the apparent atmospheric coherence time, phase-referencing promises a dramatic increase in the sensitivity of a stellar interferometer. Initial results from phase-referencing experiments at PTI are encouraging, and demonstrate that it is possible to increase coherent integration times by at least a factor of 10. We also demonstrate that phase-referenced measurements of source visibilities can be calibrated to at least the $3-7\%$ level, depending on source brightness and observing conditions. This is similar to what can be done with non-phase-referenced PTI data, and hence we see no loss of precision in using phase-referencing. Note that these data were obtained without the use of a spatial filter; adding one should improve measurement precision. Future experiments will be conducted to determine the ultimate improvement possible, as well as the effect of anisoplanatism.

Part of the work described in this paper was performed at the Jet Propulsion Laboratory under contract with the National Aeronautics and Space Administration. Funding was provided to B. F. L. through the Michelson Fellowship program. Interferometer data was obtained at the Palomar Observatory using the NASA Palomar Testbed Interferometer, supported by NASA contracts to the Jet Propulsion Laboratory. This research has made use of the Simbad database, operated at CDS, Strasbourg, France. We would like to thank C. Jones for improving the instrument interface, including audio feedback.

A. Fringe Tracking and Servos

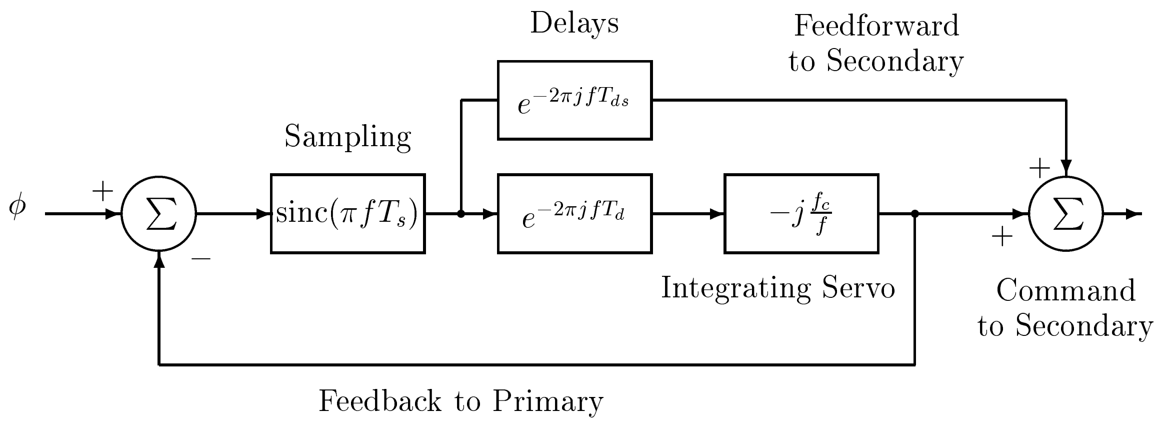

Fig. 1.— The control loop as implemented at PTI. The primary fringe tracker operates a feedback loop, while the secondary is phase-referenced. For improved performance one can also feed forward the full error signal to secondary.

The error rejection of the feedback loop for this sampled-data system can be approximated as

$$\tilde{E}_1(f) \simeq \frac{1}{1 - j\frac{f_c}{f}\mathrm{sinc}(\pi f T_s)\mathrm{e}^{-j2\pi f T_d}} \quad \text{(A1)}$$

The PSD filter function $H_{fb}(f)$ follows from

$$\begin{aligned} H_{fb}(f) &= \tilde{E}_1(f)\tilde{E}_1^*(f) && \text{(A2)} \\ &= \frac{1}{1 - 2\frac{f_c}{f}\mathrm{sinc}(\pi f T_s)\sin(2\pi f T_d) + \left(\frac{f_c}{f}\right)^2 \mathrm{sinc}^2(\pi f T_s)} && \text{(A3)} \end{aligned}$$

The error rejection of the feedforward system is approximately

$$\begin{aligned} \tilde{E}_2(f) &\simeq 1 - \frac{\mathrm{sinc}(\pi f T_s)\left(e^{-j2\pi f T_{ds}} - j\frac{f_c}{f}e^{-j2\pi f T_d}\right)}{1 - j\frac{f_c}{f}\mathrm{sinc}(\pi f T_s)e^{-j2\pi f T_d}} && \text{(A4)} \\ &= \frac{1 - \mathrm{sinc}(\pi f T_s)e^{-j2\pi f T_{ds}}}{1 - j\frac{f_c}{f}\mathrm{sinc}(\pi f T_s)e^{-j2\pi f T_d}} && \text{(A5)} \\ &= \tilde{E}_1(f)\left(1 - \mathrm{sinc}(\pi f T_s)e^{-j2\pi f T_{ds}}\right) && \text{(A6)} \end{aligned}$$

Thus $\tilde{E}_2(f)$ is the product of the feedback servo rejection function and a simple time-delay limited rejection function. When the feedback servo gain goes to 0 ($f_c \to 0$), $\tilde{E}_1(f) \to 1$ and the response is just the time-delay limited response. The PSD filter function is

$$\begin{aligned} H_{ff}(f) &= \tilde{E}_2(f)\tilde{E}_2^*(f) && \text{(A7)} \\ &= \tilde{E}_1(f)\tilde{E}_1^*(f)\left(1 - \mathrm{sinc}(\pi f T_s)e^{-j2\pi f T_{ds}}\right)\left(1 - \mathrm{sinc}(\pi f T_s)e^{+j2\pi f T_{ds}}\right) && \text{(A8)} \\ &= H_{fb}(f)\left(1 - 2\mathrm{sinc}(\pi f T_s)\cos(2\pi f T_{ds}) + \mathrm{sinc}^2(\pi f T_s)\right) && \text{(A9)} \end{aligned}$$

REFERENCES

Boden, A. F., et al., 1998, ApJ, 505, L39

Cochran W., et al., 1997,ApJ, 483, 457

Colavita, M. M., Hines, B. E., Shao, M., 1992, in ESO Conf. and Workshop Proc. 39, High Resolution Imaging by Interferometry II, ed. F. Merkle (Garching: ESO), 1143

Colavita, M. M., et al., 1994, Proc. SPIE, 2200, 89

Colavita, M. M., et al., 1999, ApJ, 510 , 505-521

Colavita, M. M., 1999, PASP, 111, 111-117

Colavita M. M., Hines, B.E., Shao, M., Klose, G. J., Gibson, B. V., 1991, Proc. SPIE, 1542, 205

Linfield, R. P., et al., 1999, Working on the Fringe: An International Conference on Optical and IR Interferometry from Ground and Space, Dana Point, CA, May 24-27, 1999. Proceedings to be published in ASP Conference Series (S. Unwin and R. Stachnik, editors), p. 58.

Shao, M., Colavita, M. M., 1992a, ARA&A, 30, 457

Shao, M., Colavita, M. M., 1992b, A&A, 262, 353

Quirrenbach, A.,et al., 1994, A&A, 286, 1019

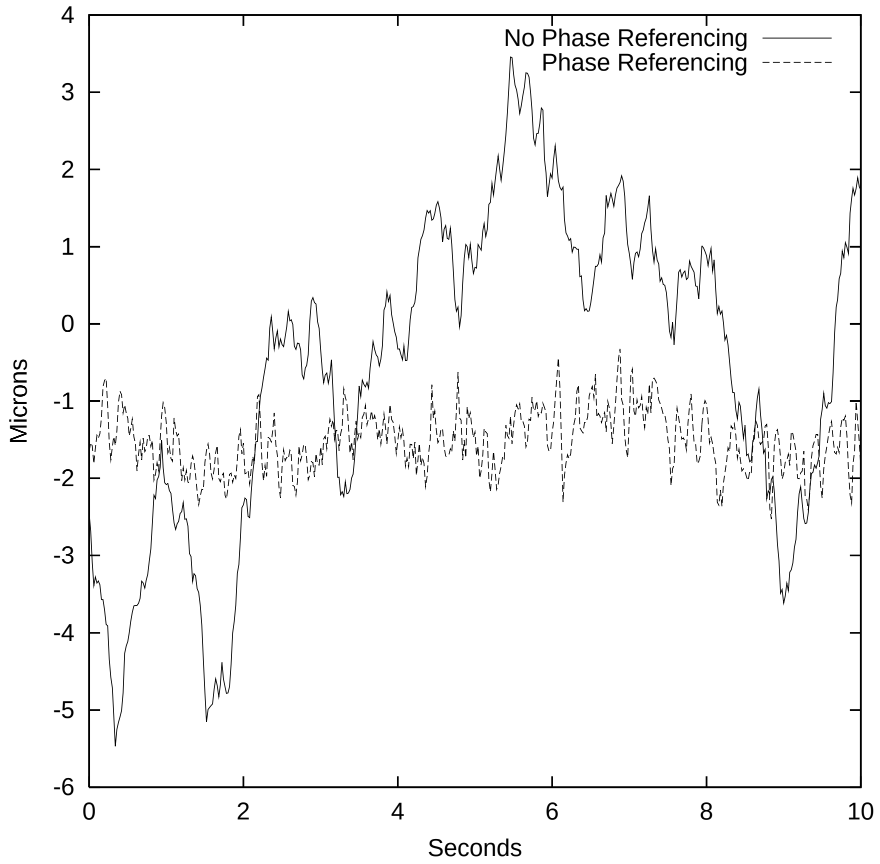

Fig. 2.— Unwrapped fringe position seen by the secondary fringe tracker with and without phase referencing. The two data sections were taken on 4 Aug, 1999, within 200 seconds of each other. The target star was HD 177724 ($m_K = 2.99$, A0V). The secondary fringe tracker was operating with 20 ms sample times and open loop, i.e., measuring but not correcting the phase.

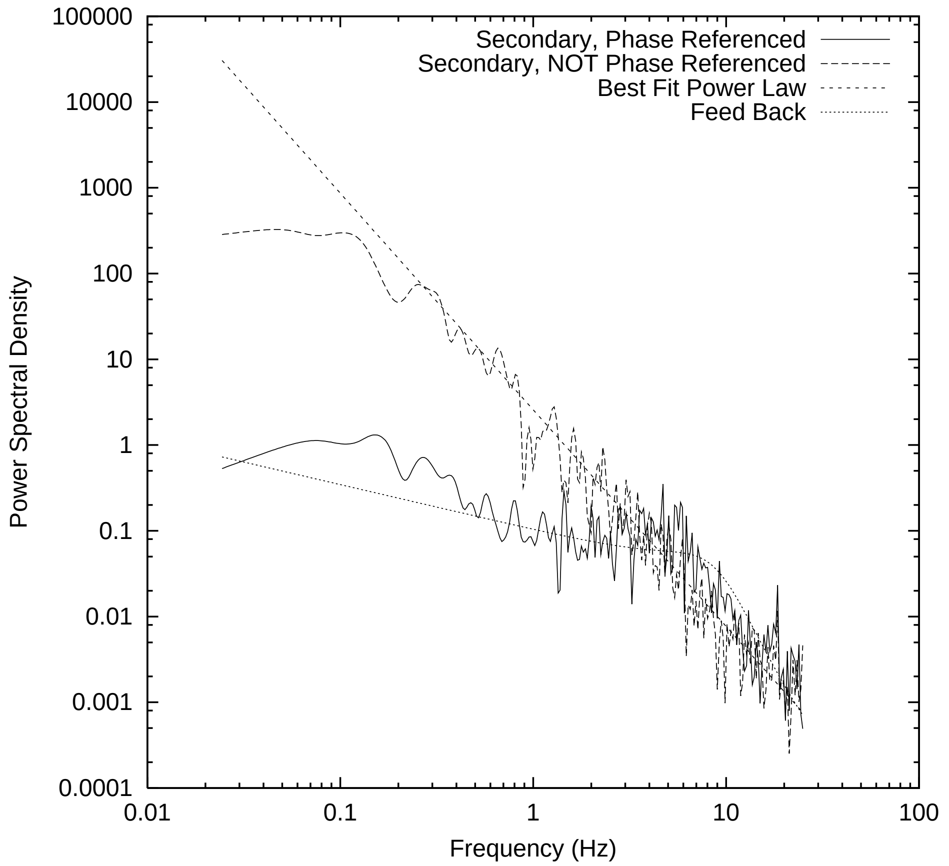

Fig. 3.— Power spectral density of the secondary phase, for both non-phase referenced and phase-referenced data. Note that the non-phase-referenced phase (essentially the atmosphere) is best fit by a power law $A(f) \propto f^{-2.5}$, somewhat shallower than the nominal -8/3 slope of Kolmogorov theory. However, it is similar to the slope seen in other PTI data (Linfield et al. 1999). Also included is the predicted power spectrum for the phase-referenced case, based on the performance of a feedback servo applied to the best-fit atmospheric power-law (see text).

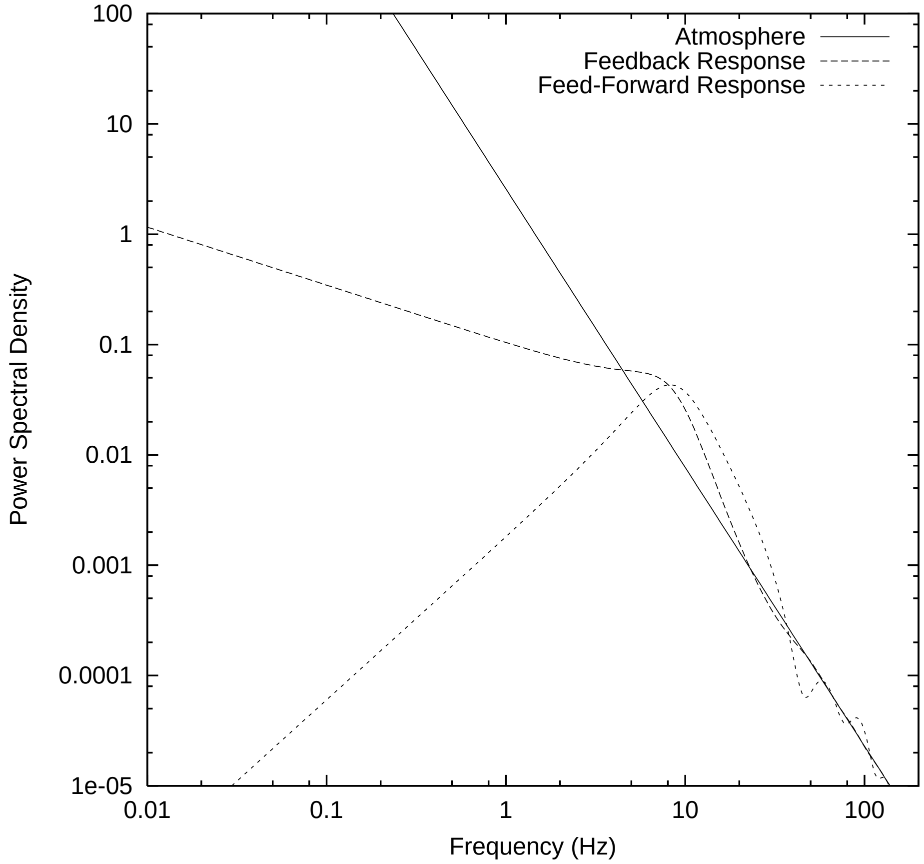

Fig. 4.— Predicted power spectra for phase referencing in the feedback and feedforward cases. The -2.5 power law is the best fit to the atmospheric power spectrum from Fig. 3., and the feedback and feedforward theoretical predictions are explained in the text. Model parameters were $f_c = 5$ Hz, $T_d = 21$ ms, $T_s = 15$ ms.

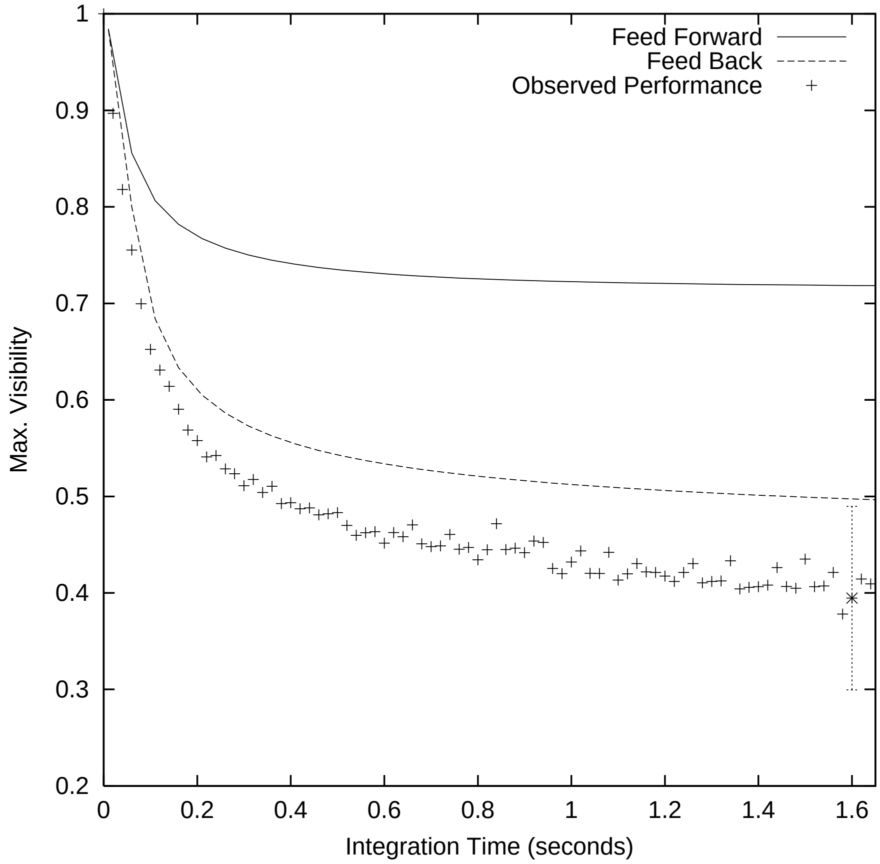

Fig. 5.— Predicted system visibility (V_{sys}^2) as a function of coherent integration time for the feedforward and feedback cases, and the observed visibility reduction obtained by averaging the time-series data shown in Figure 2. Model parameters were $f_c = 5$ Hz, $T_d = 21$ ms, $T_s = 15$ ms.

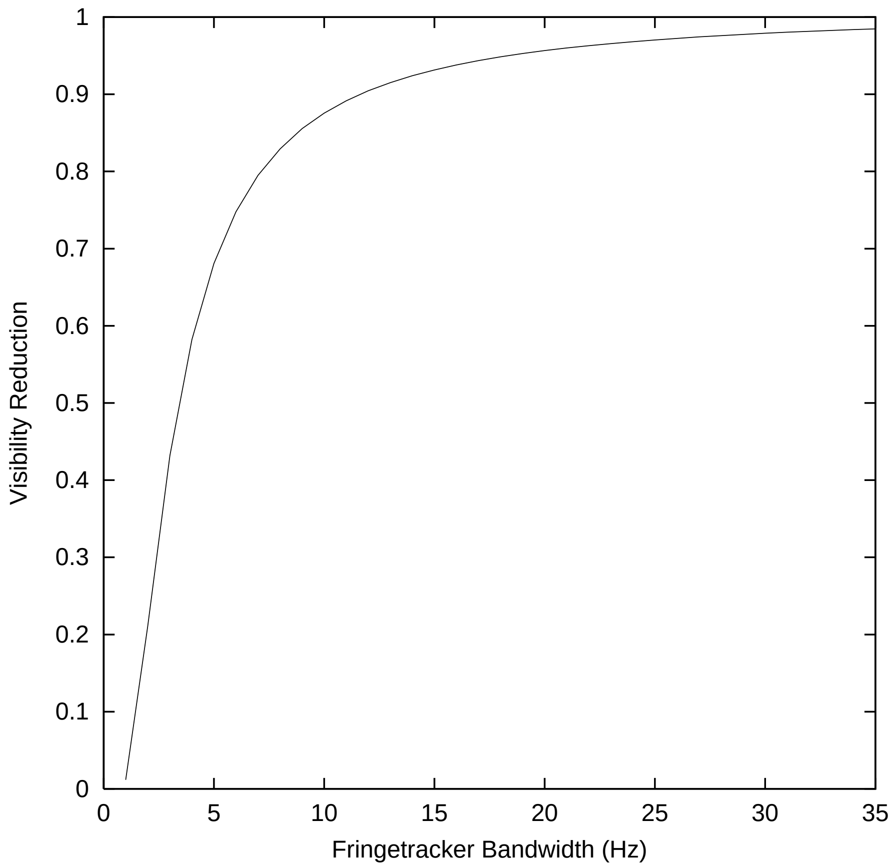

Fig. 6.— Predicted system visibility for a 2-second coherent integration time, as a function of fringe tracker closed-loop bandwidth, assuming a feed-forward servo and the PTI best-fit atmospheric power law. Model parameters were $T_d = 0.1/f_c$ and $T_s = 0.75T_d$.

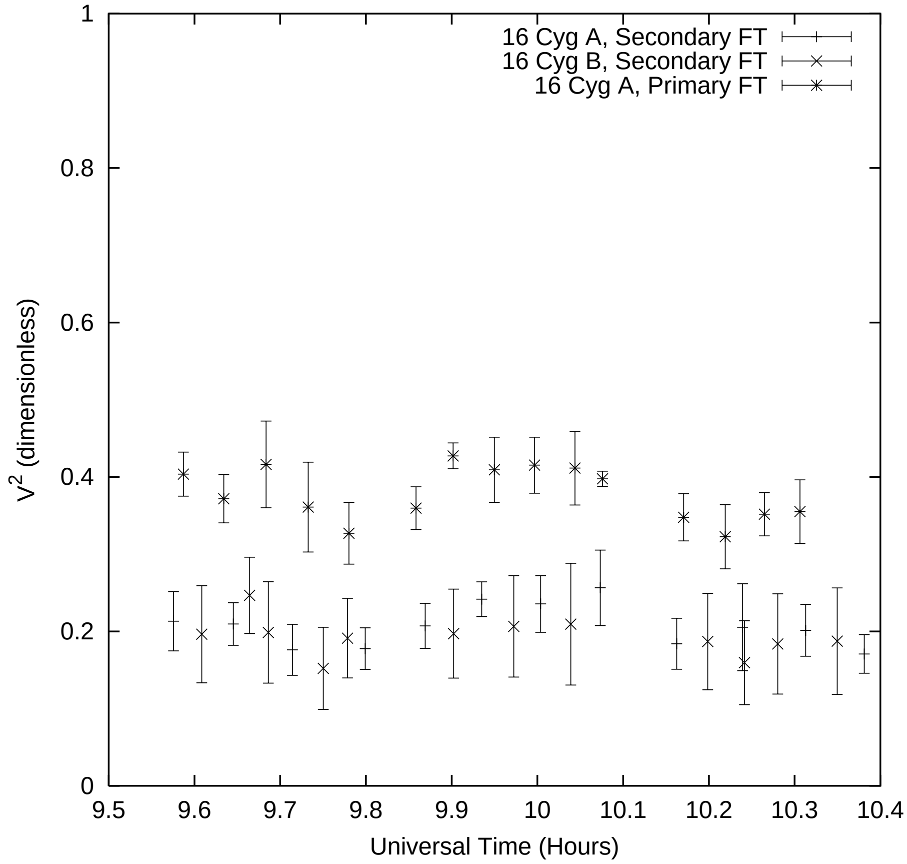

Fig. 7.— Phase-referenced visibilities of the two components of the visual binary 16 Cyg ($m_K = 4.52$, G1.5V, and $m_K = 4.65$, G3V), observed on 6 July 1999 using the broadband fringe-tracker channels. Coherent integration time was 100 ms for the secondary fringe tracker, while the primary fringe tracker used a coherent integration time of 20 ms.